A&A 408, 755–765 (2003)
DOI: 10.1051/0004-6361:20030984

Astronomy & Astrophysics

The damping of slow MHD waves in solar coronal magnetic fields

I. De Moortel and A. W. Hood

School of Mathematics and Statistics, University of St Andrews, North Haugh, St Andrews, Fife KY16 9SS, Scotland

Received 18 April 2003 / Accepted 17 June 2003

Abstract. A theoretical description of slow MHD wave propagation in the solar corona is presented. Two different damping mechanisms, namely thermal conduction and compressive viscosity, are included and discussed in detail. We revise the properties of the "thermal" mode, which is excited when thermal conduction is included. The thermal mode is purely decaying in the case of standing waves, but is oscillatory and decaying in the case of driven waves. When thermal conduction is dominant, the waves propagate largely undamped, at the slower, isothermal sound speed. This implies that there is a minimum damping time (or length) that can be obtained by thermal conduction alone. The results of numerical simulations are compared with TRACE observations of propagating waves, driven by boundary motions, and standing waves observed by SUMER/SOHO, excited by an initial impulse. For typical coronal conditions, thermal conduction appears to be the dominant damping mechanism.

Key words. Sun: corona – Sun: activity – magnetohydrodynamics (MHD)

1. Introduction

Recent observations have illustrated that the solar corona is highly dynamic. Since the launch of SOHO and TRACE, many examples of small amplitude oscillations have been detected in a variety of solar structures. Due to the high spatial and temporal resolution of these space-based missions, there are now clear examples of observations of propagating slow MHD waves, which are possibly driven by boundary motions. For example, periodic density variations in coronal plumes were first detected high above the limb by Ofman et al. (1997) using the white light channel of UVCS/SOHO. DeForest & Gurman (1998) detected quasi-periodic, propagating intensity disturbances in EIT/SOHO observations of polar plumes. Ofman et al. (1999, 2000) found that these quasi-periodic disturbances could be modelled as slow magneto-acoustic waves. Non-linear, two-dimensional MHD simulations show that the outward-propagating slow waves steepen non-linearly and may contribute significantly to the heating of the corona by viscous dissipation. Using EIT/SOHO and TRACE respectively, Berghmans & Clette (1999) and De Moortel et al. (2000) reported on the detection of similar propagating oscillations observed in coronal loops, whereas Robbrecht et al. (2001) compare propagating disturbances in coronal loops in the EIT/SOHO 195 Å and TRACE 171 Å passbands. Based on these observations, Nakariakov et al. (2000) presented a model, again in terms of slow magneto-acoustic waves, and concluded that the main factors influencing the wave evolution are dissipation and stratification. The model was further developed by Tsiklauri & Nakariakov (2001), who incorporated the effect of a non-zero inclination angle and a semi-circular loop offset. An extensive overview of longitudinal intensity oscillations observed in coronal loops, together with a discussion of the measured parameters was recently presented by De Moortel et al. (2002a,b). Using a combination of different instruments, a number of authors have recently found evidence for the propagation of slow magneto-acoustic waves through the transition region and into the corona. Using mainly CDS/SOHO, MDI/SOHO and TRACE, O'Shea et al. (2002) found oscillations present in a sunspot umbra at all investigated temperatures, from the temperature minimum (TRACE 1700 passband) to the coronal temperature of $\log T = 6.4$ (CDS FE XVI 335 Å). The measured propagation speeds suggest that the observed oscillations are slow magneto-acoustic waves propagating from the footpoints along the magnetic field lines. From a joint SOHO and TRACE observing campaign, Brynildsen et al. (2002) also found evidence for a 3 min period oscillation above a sunspot umbra. The oscillation amplitudes are found to increase with increasing temperature, reaching a maximum at about $1–2 \times 10^5$ K and then decreasing again in the higher temperature lines. These authors again suggest that wave propagation along the magnetic field above a sunspot region makes it possible for the 3 min oscillations to reach the corona. De Moortel et al. (2002c) presented results that indicate that not only the 3-min (umbral) oscillation but also oscillations with a 5 min period are observed in the corona.

Recently, a totally different class of observed oscillatory phenomena, namely flare-excited, transversal oscillations of coronal loops have been the subject of considerable debate. Using TRACE observations, Schrijver et al. (1999), and subsequently Aschwanden et al. (1999), were first to present evidence of transversal oscillations of active region loops.

Send offprint requests to: I. De Moortel,
e-mail: ineke@mcs.st-and.ac.uk

The oscillations, with a period of roughly 5 min, are excited by flares and decay extremely rapidly, on a timescale of the order of 15 min. Using the same set of observations, Nakariakov et al. (1999) suggested that the dissipation coefficient in the corona could be as much as eight or nine orders of magnitude larger than the theoretically predicted classical value. However, from a different set of observed loop oscillations, Schrijver & Brown (2000) argue that rocking motions in the photosphere, associated with the flare, cause the loops to oscillate and thus that the observed damping will only contain information about photospheric properties, rather than coronal properties.

The detection of oscillations in the solar corona can be used to improve existing estimates of coronal properties and dissipation coefficients, both from direct measurements and indirect methods such as "coronal seismology". The idea of using observed oscillations as a diagnostic tool for determining physical conditions of the coronal plasma was first suggested almost two decades ago by Roberts et al. (1984). However, only now do we see the first results of this idea, due to the increased temporal and spatial resolution of present-day, spaced-based observations. Indeed, using the idea of coronal seismology, Nakariakov & Ofman (2001) discuss the possibility of determining the Alfvén speed and magnetic field strength in coronal loops from observed, flare-generated, transversal oscillations. The possible role of leakage of the wave energy at the footpoints of the oscillating loops as a mechanism for the observed rapid damping is studied by De Pontieu et al. (2001) and Ofman (2002). Different damping mechanisms are presented by Ofman & Aschwanden (2002), who suggest that the loop oscillations are dissipated by phase mixing with anomalously high viscosity and Ruderman & Roberts (2002), who present an alternative model in terms of resonant absorption to explain the strong damping of the transversal loop oscillations. Goossens et al. (2002) show that resonant absorption of quasi-mode kink oscillations can account for the observed rapid damping if the ratio of the length scale of the inhomogeneity to the radius of the loop is allowed to vary from loop to loop. This interpretation explains the rapid damping without the need to invoke anomalously low Reynolds numbers. An extensive overview and analysis of a large number of transversal coronal loop oscillations was presented by Schrijver et al. (2002) and a detailed discussion of the parameters obtained from these observations can be found in Aschwanden et al. (2002). These authors suggest that the observed, transversal loop oscillations conform to some extent to the evolution of impulsively generated MHD waves, where the rapid decay time could be explained by a realistic treatment of the leakage of wave energy at the footpoints of the loops.

Analysing SUMER/SOHO observations of a solar limb flare, Kliem et al. (2002) and Wang et al. (2002a) found rapidly damped, oscillatory Doppler shifts, where the large initial disturbance points toward a similar interpretation in terms of impulsively generated MHD waves. Due to the good agreement with the observed periods (~14–18 min) Wang et al. (2002b) favour an interpretation in terms of a slow standing wave, although they do point out that the absence of brightness fluctuations with the same oscillatory period argues against a compressive wave. The results of one dimensional, non-linear MHD simulations, including thermal conduction and compressive viscosity, strongly suggest that the observed Doppler shift oscillations are indeed signatures of damped slow magnetosonic waves (Ofman & Wang 2002). The large thermal conduction due to the high temperatures is the dominant wave damping mechanism, with a less significant contribution from compressive viscosity.

In this paper, we investigate the properties of uncoupled slow MHD waves, from the point of view of boundary driven oscillations. A theoretical study of the properties of MHD waves can be found in e.g. Porter et al. (1994a,b) and Roberts (2000). The key features in our simulations are the damping of the waves due to two possible mechanisms, namely thermal conduction and viscosity. We point out that thermal conduction introduces an extra "thermal" mode, in addition to the slow mode (see Field 1965). After a description of the basic equations (Sect. 2) and an investigation of the effect of varying the dimensionless parameters (Sect. 3), specific observations are modelled (Sect. 4). Conclusions are summarised in Sect. 5.

2. Basic equations

In this work we only consider the slow MHD oscillations and so restrict attention to motions along the background magnetic field, directed along the z-axis. Thus, the MHD equations reduce to a 1D system of the form

$$\rho\frac{\partial v}{\partial t}+\rho v\frac{\partial v}{\partial z}=-\frac{\partial p}{\partial z}+\frac{4}{3}\eta_0\frac{\partial^2 v}{\partial z^2}, \tag{1}$$

$$\frac{\partial \rho}{\partial t}=-\frac{\partial}{\partial z}\left(\rho v\right), \tag{2}$$

$$\frac{\partial p}{\partial t}+v\frac{\partial p}{\partial z}=-\gamma p\frac{\partial v}{\partial z}+(\gamma-1)\frac{\partial}{\partial z}\left(\kappa_{\parallel}\frac{\partial T}{\partial z}\right), \tag{3}$$

$$p=\frac{1}{\tilde{\mu}}\rho RT. \tag{4}$$

ρ is the mass density, p the gas pressure, T the temperature, v the velocity parallel to the magnetic field, $\eta_0 = 10^{-17}T^{5/2}$ kg m^{-1} s^{-1} (Hollweg 1985; Hood et al. 1989) the viscosity parallel to the magnetic field (the compressive viscosity), $\kappa_{\parallel} = \kappa_0 T^{5/2}$ W m^{-1} deg^{-1} the thermal conductivity parallel to the magnetic field, R the gas constant and $\tilde{\mu}$ the mean molecular weight. The basic equilibrium is taken as a uniform plasma with pressure, p_0, density, ρ_0, and temperature, T_0. Due to thermal conduction, we consider the background temperature to be almost isothermal and hence neglect both optically thin radiation and the unknown coronal heating function.

Before proceeding, Eqs. (1) to (4) are made dimensionless using the equilibrium values for pressure, density and temperature. The velocity is expressed as $v = c_s\bar{v}$, where the adiabatic sound speed, c_s is defined by

$$c_s^2=\frac{\gamma p_0}{\rho_0}. \tag{5}$$

For future reference, the isothermal sound speed is defined by

$$c_i^2=\frac{p_0}{\rho_0}. \tag{6}$$

The length and time are non-dimensionalised in terms of a distance L and time τ, where

$$L = c_s \tau.$$

The resulting system of equations contains the following dimensionless parameters, namely the Reynolds number, R,

$$\epsilon = \frac{1}{R} = \frac{\eta_0 \tau}{\rho_0 L^2}, \tag{7}$$

and the thermal ratio, defined in De Moortel et al. (2002b) as

$$d = \frac{(\gamma - 1)\kappa_{\|} T_0 \rho_0}{\gamma^2 p_0^2 \tau} = \frac{1}{\gamma} \frac{\tau_s}{\tau_{\rm cond}}, \tag{8}$$

which is the ratio of the sound travel time ($\tau_s = L/c_s$) and the thermal conduction timescale ($\tau_{\rm cond} = L^2 p_0/(\gamma - 1)\kappa_{\|} T_0$). Notice that ϵ and d are expressed in terms of the timescale τ. This is preferrable since most observed waves have a prescribed period, which we take as τ, rather than a prescribed coronal loop length.

Dropping bars from dimensionless quantities, Eqs. (1) to (4) are linearised to give

$$\frac{\partial v_1}{\partial t} = -\frac{1}{\gamma}\frac{\partial p_1}{\partial z} + \frac{4}{3}\epsilon \frac{\partial^2 v_1}{\partial z^2}, \tag{9}$$

$$\frac{\partial \rho_1}{\partial t} = -\frac{\partial v_1}{\partial z}, \tag{10}$$

$$\frac{\partial T_1}{\partial t} = -(\gamma - 1)\frac{\partial v_1}{\partial z} + \gamma d \frac{\partial^2 T_1}{\partial z^2}, \tag{11}$$

$$p_1 = \rho_1 + T_1. \tag{12}$$

Consider the case $\epsilon = 0$. If the thermal ratio d is also zero, then the linearised equations simply reduce to sound waves that propagate with the adiabatic sound speed. Intuitively, one would imagine that the inclusion of thermal conduction will introduce dissipation and that the disturbances will automatically be damped. This is certainly true if d is small. However, if d is very large, then Eq. (11) implies that $T_1 = 0$ and Eq. (12) gives $p_1 = \rho_1$ so that Eqs. (9) and (10) give undamped sound waves that propagate at the isothermal sound speed, $c_i = c_s/\sqrt{\gamma}$. Therefore, if thermal conduction dominates ($d \gg 1$) then disturbances are simply undamped waves that propagate at a slower speed. Notice that the velocity is always damped if viscosity is included. However, the rate at which the disturbances damp in relation to the period of the oscillations depends on the value of the non-dimensional parameter ϵ.

2.1. Boundary conditions

Finally, a discussion of boundary conditions is important. The observations of De Moortel et al. (2002a,b) show that slow waves are propagating in from the footpoints of coronal loops. In this case driven boundary conditions are necessary. Thus, for the driven case we consider the initial conditions

$$v_1(z,0) = p_1(z,0) = \rho_1(z,0) = T_1(z,0) = 0, \tag{13}$$

and the boundary conditions

$$v_1(0,t) = f(t), \qquad \frac{\partial p_1}{\partial z}(0,t) = -f'(t), \tag{14}$$

and

$$v_1(z_{\rm max},t) = 0, \quad \frac{\partial p_1}{\partial z}(z_{\rm max},t) = 0. \tag{15}$$

Notice that in the ideal case, when $\epsilon = d = 0$, only the velocity conditions are necessary and that pressure conditions are simply consistent with the linearised equations. A standing wave problem can be modelled by assuming that $f(t) = 0$ above and the initial conditions are

$$v_1(z,0) = F(z), \quad p_1(z,0) = \rho_1(z,0) = T_1(z,0) = 0. \tag{16}$$

The actual choices for $f(t)$ and $F(z)$ will be specified later. Additionally, the temperature conditions must be selected. Two obvious choice are zero temperature, so that

$$T_1(0,t) = T_1(z_{\rm max},t) = 0, \tag{17}$$

and zero flux where

$$\frac{\partial T_1}{\partial z}(0,t) = \frac{\partial T_1}{\partial z}(z_{\rm max},t) = 0. \tag{18}$$

In the first case, thermal energy flows out through the ends of the loop whereas in the second case heat does not escape from the system. In general, the choice of temperature boundary conditions is not too critical for damped oscillations. It can make the difference between stable and unstable modes when the equilibrium temperature is not uniform (see, for example, Hood & Priest 1980). For the simulations presented in the rest of this paper, we select the first temperature condition, given in Eq. (17). The partial differential equations will be solved using a simple, second-order, Lax-Wendroff scheme.

3. Theoretical considerations

Before presenting the results of the numerical simulations, we investigate the infinite uniform medium using the results of Field (1965). Assume that all disturbances are expressed as Fourier components, $\exp \mathrm{i}(\omega t - kz)$, and that viscosity is neglected, so that thermal conduction is the only damping mechanism. Thus, a dispersion relation is obtained that is quartic in the wavenumber k and cubic in the frequency ω,

$$\omega^3 - \mathrm{i}\omega^2 \gamma d k^2 - \omega k^2 + \mathrm{i} d k^4 = 0. \tag{19}$$

For a fixed wavenumber, as in the case of standing waves, the three values of ω correspond to two slow waves modified by thermal conduction and a purely imaginary solution, giving a decaying disturbance in time, denoted as the "thermal" mode. Note that for $d = 0$ we have $\omega = \pm k$ and for $d \to \infty$, $\omega = \pm k/\sqrt{\gamma}$ as described above. To avoid having to specify a value for the wavenumber k, we re-write Eq. (19) in terms of ω/k and kd. We remind the reader that all variables are dimensionless. The slow waves have a minimum damping time as can be seen in Fig. 1a, where the dimensionless damping time, which is proportional to the reciprocal of the imaginary part of ω/k, is plotted against kd. Thus, if the required damping time for observed slow waves is shorter than the minimum thermal conduction damping time, then another damping mechanism is required. The damping per period, introduced by

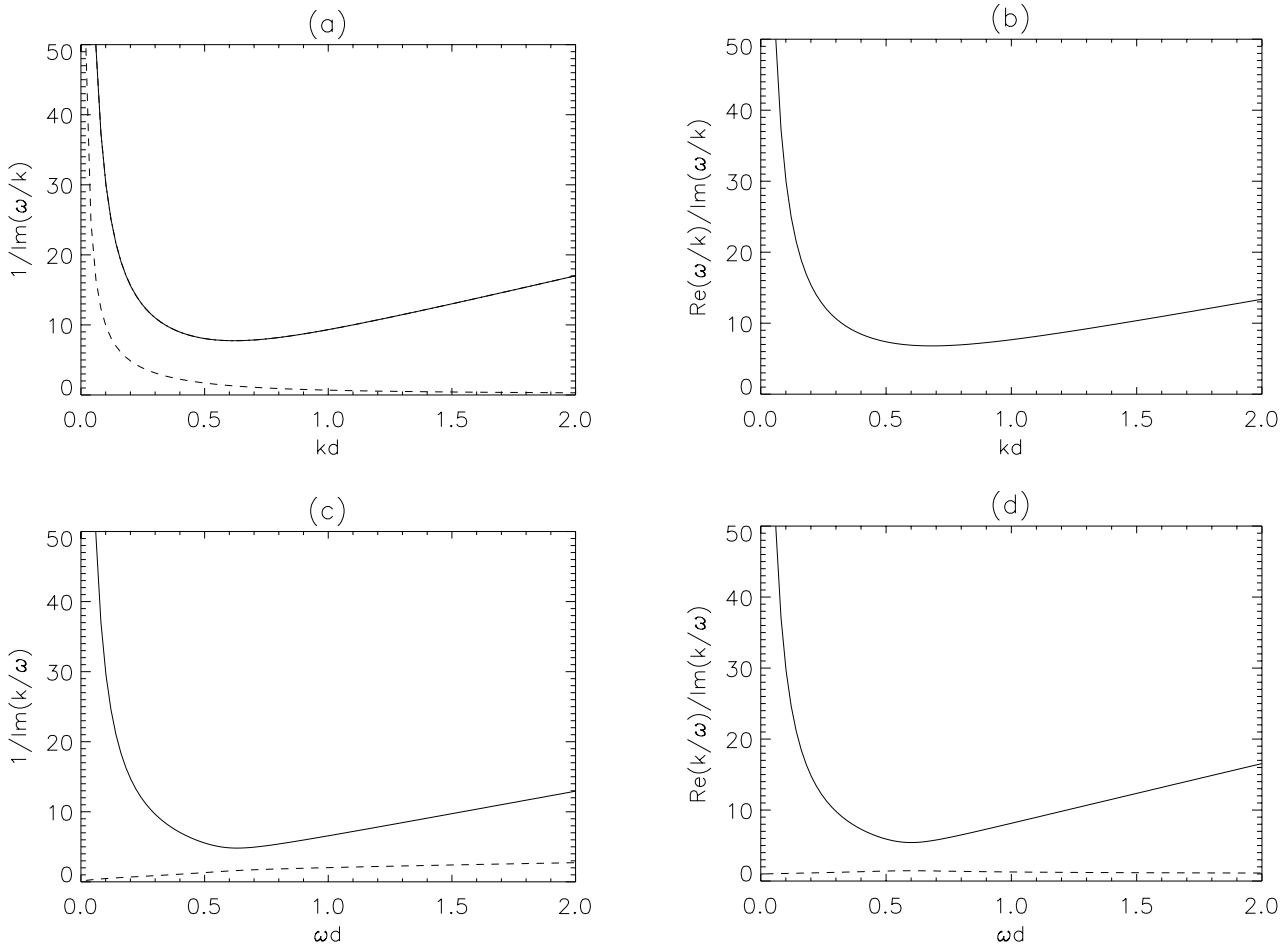

Fig. 1. The variation of **a)** the damping time $\mathrm{Im}(\omega/k)^{-1}$ and **b)** $D_{\mathrm{p},\omega} = \mathrm{Re}(\omega/k)/\mathrm{Im}(\omega/k)$ as a function of kd. **c)** The variation of the damping length $\mathrm{Im}(k/\omega)^{-1}$ and **d)** $D_{\mathrm{p,k}} = \mathrm{Re}(k/\omega)/\mathrm{Im}(k/\omega)$ as a function of ωd. The solid line corresponds to the slow mode, whereas the dashed line corresponds to the thermal mode.

Stein & Spiegel (1967), is defined as $D_{\mathrm{p},\omega} = \mathrm{Re}(\omega/k)/\mathrm{Im}(\omega/k)$ and gives a measure of the number of oscillations before the wave is damped. This can be obtained from observations and compared with the theoretical models. As the thermal mode is purely imaginary, $D_{\mathrm{p},\omega}$ is of course only plotted for the slow waves in Fig. 1b. Again, if the observed number of periods is less than the minimum number of periods before the wave is damped due to thermal conduction, an additional damping mechanism will be needed.

The driven boundary case can be considered by assuming that the frequency is fixed. As Eq. (19) is quartic in the wavenumber k, there will be four solutions, corresponding to two slow waves, and two thermal modes. Contrary to the standing waves, both the slow and thermal mode are now oscillatory and decaying in height. This time, to avoid having to specify a value for the frequency ω, we re-write Eq. (19) in terms of k/ω and ωd. The dimensionless damping length is then proportional to the reciprocal of the imaginary part of k/ω, and is plotted in Fig. 1c. The slow waves have a minimum damping length due to thermal conductivity. If the damping length observed is shorter than the minimum damping length predicted by thermal conductivity, then the waves must be damped by some other mechanism. Finally, the damping per wavelength, $D_{\mathrm{p,k}} = \mathrm{Re}(k/\omega)/\mathrm{Im}(k/\omega)$ is shown in Fig. 1d. $D_{\mathrm{p,k}}$ is plotted for both the slow mode and the thermal mode, seeing that the latter is now oscillatory. It is clear that the thermal mode is damped extremely quickly, and that very few oscillations would be observed.

3.1. Slow mode propagation (ideal case)

In this section, the behaviour of slow waves that are driven by boundary conditions at $z = 0$ is considered by selecting the forcing function $f(t)$. For a monochromatic source, we take

$$f(t) = \begin{cases} \sin 2\pi t & 0 < t < n, \\ 0 & \text{elsewhere}, \end{cases} \tag{20}$$

where n defines the number of cycles that the boundary is driven for. For large n, the boundary is effectively driven harmonically. More random driving can be selected by choosing an appropriate form for $f(t)$.

Before considering the damping due to thermal conduction, it is appropriate to revise some of the ideas of slow mode propagation (Roberts 1985 and references therein). If the length of the loop, in dimensionless units, is an integer multiple of 0.5, then the loop will resonate, with the amplitude of the velocity

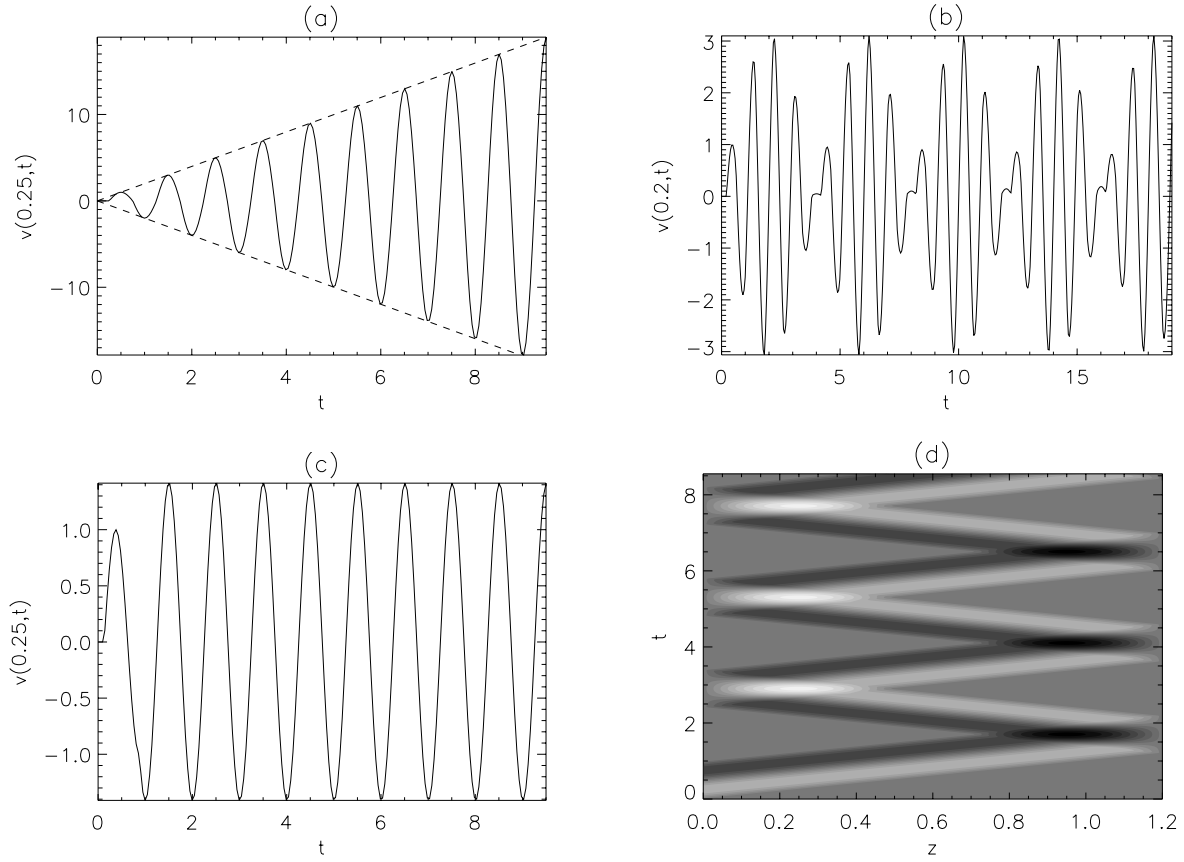

Fig. 2. a) A cross-section of the perturbed velocity as a function of time at $z = 0.25$, for which $z_{\max} = 0.5$ and $d = \epsilon = 0$ and for which the boundary was driven continuously. **b)** A similar cross-section of the velocity at $z = 0.2$, with $z_{\max} = 0.4$. **c)** A cross-section of the perturbed velocity at $z = 0.25$ in a loop driven for only one cycle, with $z_{\max} = 0.5$ and $d = \epsilon = 0$. **d)** Contour plot of the velocity as a function of z and t in a loop driven for only one cycle with $z_{\max} = 1.2$.

growing linearly with time. In Fig. 2a, a cross-section of the velocity at $z = 0.25$, for which $z_{\max} = 0.5$, is shown as a function of time t. The dashed lines illustrate that the amplitude of the perturbed velocity does indeed increase linearly with time. Detuning the loop by decreasing the length from $z_{\max} = 0.5$ to $z_{\max} = 0.4$ produces a velocity pattern that oscillates with the driving frequency but has an amplitude that is modified by a beat frequency. This is illustrated in Fig. 2b, where a cross-section of the velocity at $z = 0.2$ is plotted. In both cases, the boundary was driven continuously throughout the simulation, producing, in effect, harmonically driven waves. Next, we consider a boundary driving motion that consists of only one period. If the loop is resonant, for example taking $z_{\max} = 0.5$, a standing wave is created but if the loop is non-resonant, e.g. $z_{\max} = 1.2$, a propagating disturbance, which travels without changing shape, is produced. These results are clearly shown in Figs. 2c and d.

3.2. Thermal conduction

We now repeat the previous simulations but include dissipation through thermal conduction. It is easy to demonstrate that, under the assumption of a single fluid, so that $T = T_{\rm e} = T_{\rm p}$, the ratio of the electron and ion thermal conductivity, $\kappa_{\parallel}^{\rm e}/\kappa_{\parallel}^{\rm i} \sim \sqrt{m_{\rm i}/m_{\rm e}}$, where $m_{\rm i}$ and $m_{\rm e}$ are the ion and electron mass, respectively. This implies that thermal conductivity along the magnetic field will be primarily by electrons. Using Eq. (8) and assuming standard coronal values for all variables,

$$\begin{cases} T_0 = 10^6 \text{ K}, \\ \rho_0 = 1.67 \times 10^{-12} \text{ kg m}^{-3}, \\ \kappa_{\parallel} = 10^{-11}\, T_0^{5/2} \text{ W m}^{-1} \text{ deg}^{-1}, \\ \tilde{\mu} = 0.6, \\ \mathcal{R} = 8.3 \times 10^3 \text{ m}^2 \text{ s}^{-2} \text{ deg}^{-1}, \\ \gamma = 5/3, \\ \tau = 300 \text{ s}, \end{cases} \tag{21}$$

gives a value of $d = 0.025$ for the thermal ratio. Using this value for d in our simulations, Fig. 3a shows a cross-section at $z = 0.25$ of the perturbed velocity, as a function of time, driven with an infinite harmonic wavetrain. When the loop is resonantly driven, e.g. with $z_{\max} = 0.5$ (solid line), the amplitude initially increases, as the fundamental, resonant mode is excited. However, thermal conduction stops this growth and the amplitude levels off as a steady state is reached, whereby the energy being injected into the system through the boundary motions balances the energy leaving the system. The dashed line shows the result of thermal conduction on a non-resonant loop. Here $z_{\max} = 0.6$ and instead of driving a resonance, there is some evidence of an initial growth and the start of the beat phenomena, but the amplitude rapidly reaches a constant value

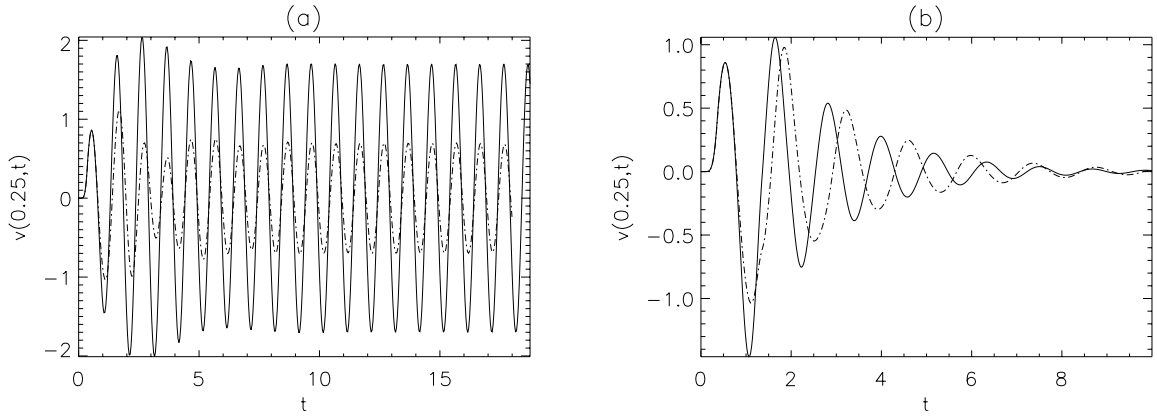

Fig. 3. a) A cross-section of the perturbed velocity as a function of time at $z = 0.25$, for which $z_{\max} = 0.5$, $d = 0.025$, $\epsilon = 0$ and for which the boundary was driven continuously. The dashed line shows the result for the not-resonantly driven loop with $z_{\max} = 0.6$. **b)** Similar to **a)** but for a loop driven for only one cycle.

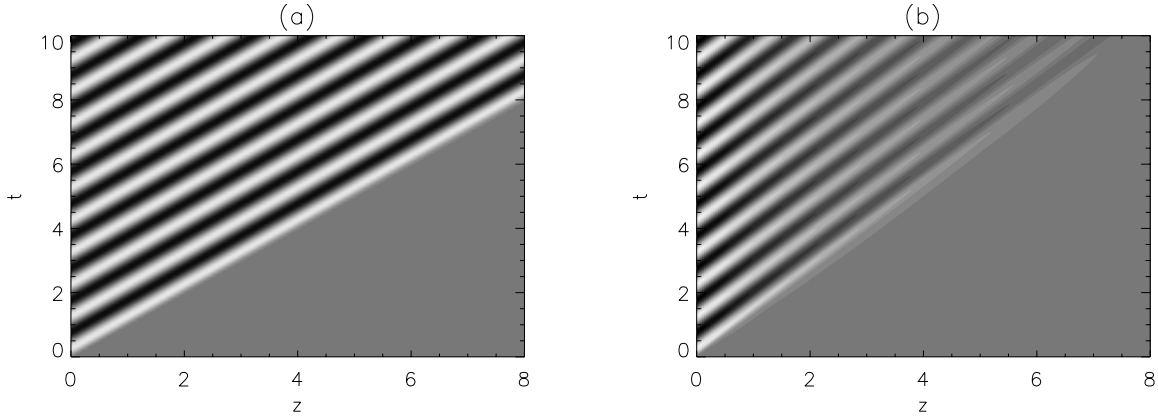

Fig. 4. a) Contour plot of the perturbed velocity as a function of z and t, for which $z_{\max} = 15$ and $d = \epsilon = 0$ and for which the boundary was driven continuously. **b)** Similar to **a)** but with $d = 0.48$.

that is considerably smaller than in the resonant case. Figure 3b shows the behaviour when only one cycle of the boundary motion occurs. For the resonant loop case, $z_{\max} = 0.5$ (solid line), a standing wave is created, which damps as expected. For $z_{\max} = 0.6$ (dashed line) a disturbance that is made up of many of the harmonics of standing modes is produced. There is an initial rapid decay as the higher harmonics decay faster before the fundamental mode emerges and decays in a similar manner as the resonant case.

If we compare the results for the slow mode propagation in an ideal plasma (Fig. 2) with the wave propagation when thermal conduction is included (Fig. 3), it is clear that the amplitudes of the waves are considerably smaller due to the thermal conduction. The immediate thought is that, since thermal conduction can damp these disturbances, increasing the thermal conductivity through an increase in the thermal ratio should result in the required damping rate to match with observations. However, as mentioned in the discussion of Eqs. (9)–(12), there is a minimum decay length and time. For very small values of d, the slow waves travel undamped at the adiabatic sound speed, which in our dimensionless units has been normalised to one. In the limit of large d they are only weakly damped and travel at the isothermal sound speed, which has been normalised to $1/\sqrt{\gamma}$. This is shown in the simulations of slow waves propagating in from one footpoint, for which the upper boundary $z_{\max}$ was taken sufficiently large, so that the waves do not reach this boundary within the duration of the simulation. Figure 4a shows a contour plot of the resulting perturbed velocity, when no thermal conduction is present, i.e. $d = 0$. At a time $t = 8$, the perturbations reach a position $z = 8$, confirming that the dimensionless wavespeed is equal to one. However, when a large amount of thermal conductivity is present, e.g. $d = 0.48$, the gradients of the diagonal slopes in the contour plot of the velocity (Fig. 4b) become steeper, indicating that the waves are travelling slower. Indeed, at a time $t = 8$, the perturbations only reach a position $z \approx 6.15 = 8/\sqrt{\gamma}$. Increasing the thermal conductivity even further results in perturbations that travel more or less undamped at a dimensionless speed $1/\sqrt{\gamma}$. These simulations also confirmed that for large d, the amplitudes of the temperature perturbations T_1 are very small, and thus, that the plasma has effectively become isothermal. As predicted by Eq. (12), the perturbed pressure p_1 and density ρ_1 have roughly the same amplitudes. In the ideal case, there are significant temperature perturbations, and consequently, the pressure perturbations are larger than the density perturbations.

Additionally, the different propagation speed results in a different resonant behaviour. Now loops with a dimensionless length that is an integer multiple of $0.5/\sqrt{\gamma} \approx 0.4$ will

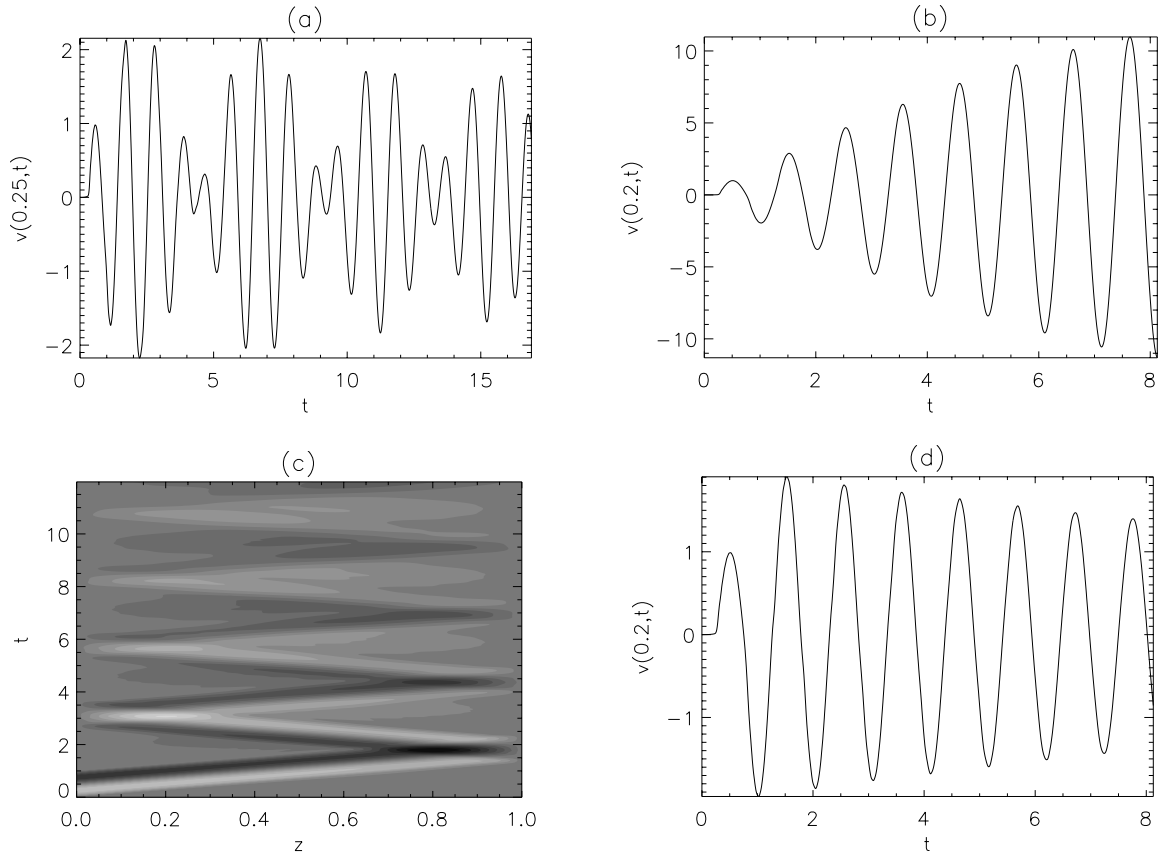

Fig. 5. a) A cross-section of the perturbed velocity as a function of time at $z = 0.25$, for which $z_{\max} = 0.5$, $d = 0.48$, $\epsilon = 0$ and for which the boundary was driven continuously. **b)** A similar cross-section of the velocity at $z = 0.2$, with $z_{\max} = 0.4$. **c)** Contour plot of the velocity as a function of z and t in a loop driven for only one cycle, with $z_{\max} = 1.0$, $d = 0.48$, $\epsilon = 0$. **d)** A cross-section of the perturbed velocity at $z = 0.2$ in a loop driven for only one cycle, with $z_{\max} = 0.4$, $d = 0.48$, $\epsilon = 0$.

resonate. Indeed, Fig. 5a shows that a harmonically driven loop, with length $z_{\max} = 0.5$ now produces a perturbed velocity that oscillates with the driving frequency but has an amplitude that is modulated by a beat frequency. The amount of thermal conductivity that is present still produces a small amount of damping. Choosing an even larger value for the thermal ratio d will result in a velocity pattern that is qualitatively similar to the velocity oscillations seen in a non-resonant loop in an ideal plasma (see Fig. 2b). Tuning the loop to be resonant by choosing $z_{\max} = 0.4$ results in the amplitude of the velocity growing with time. The growth rate is slower than linear, as the perturbations are still slightly damped due to the thermal conduction. Figures 5c, d show that driving the boundary for only one cycle produces similar results as before. If the loop is non-resonant, for example taking $z_{\max} = 1.0$, a propagating pulse is created, whereas in a resonant loop, e.g. $z_{\max} = 0.4$, a standing wave is excited. There is again still a small amount of damping present in both cases.

3.3. Viscosity

In this section, we investigate the effect of compressive viscosity on the damping of slow waves, and compare it with the damping due to thermal conduction. Contrary to thermal conductivity, the ratio of electron and ion viscosity, $\eta_0^{\rm e}/\eta_0^{\rm i} \sim \sqrt{m_{\rm e}/m_{\rm i}}$ and thus, ion viscosity will give by far the dominant contribution. Using Eq. (7), the values quoted in Eq. (21) and $\eta_0 = 10^{-17}\ T^{5/2}$ kg m^{-1} s^{-1}, we find a value of $\epsilon = 0.00086$ for the dimensionless viscosity coefficient. For such a small value of ϵ, the effect of compressive viscosity is hardly noticeable and therefore, we will use an artificial value, which is roughly ten times larger, $\epsilon = 0.0075$. The results of the simulations are illustrated in Figs. 6a, b. When the boundary is driven with an infinite harmonic wavetrain (Fig. 6a), the amplitude of the perturbed velocity initially increases but due to the viscosity, the amplitudes level off and eventually, a steady state is achieved, whereby the incoming and outgoing energy balance each other. The dashed line shows the result in a non-resonant loop, i.e. $z_{\max} = 0.6$. Initally, a beat frequency appears but very quickly, the amplitudes are levelled out by the viscosity. When the boundary is driven for only one cycle (Fig. 6b), only a limited amount of energy is injected into the system and the perturbations are damped. The results for $\epsilon = 0.075$, i.e. about 100 times the theoretically predicted value, are shown in Figs. 6c, d. Generally, there is little difference between the evolution of the perturbations in a resonant or in a non-resonant loop as the perturbations are damped before the resonant effects can become significant. Comparing with Fig. 3 shows that the behaviour of the perturbations is very similar whether

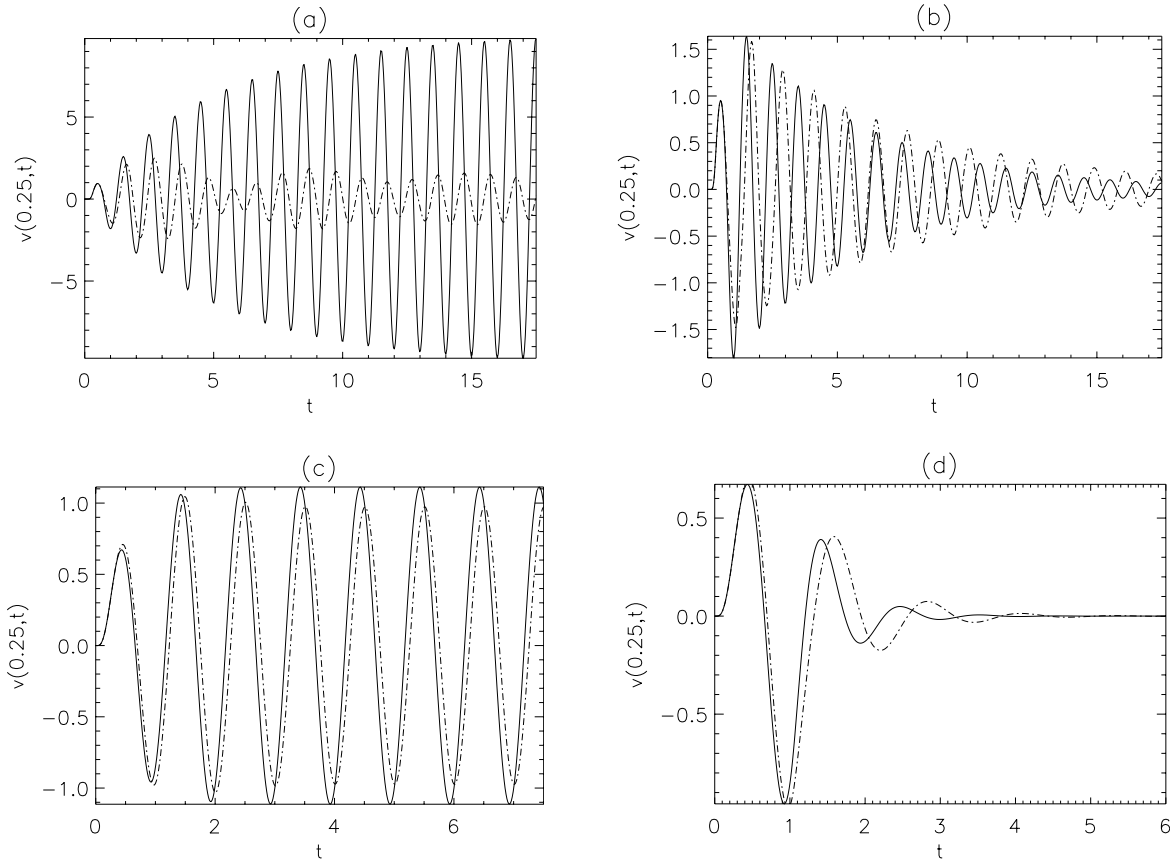

Fig. 6. a) A cross-section of the perturbed velocity as a function of time at $z = 0.25$, for which $z_{\max} = 0.5$, $\epsilon = 0.0075$, $d = 0$ and for which the boundary was driven continuously. The dashed line shows the result for the not-resonantly driven loop with $z_{\max} = 0.6$. **b)** Similar to **a)** but for a loop driven for only one cycle. **c)** Similar to **a)** but with $\epsilon = 0.075$. **d)** Similar to **b)** but with $\epsilon = 0.075$.

"normal" thermal conductivity or a lot of compressive viscosity is present. Keeping in mind that we enhanced the value of ϵ by a factor of ten to one hundred, we expect thermal conduction to be the dominant damping mechanism of slow waves in coronal loops, and the contribution of compressive viscosity to be less significant. However, we remind the reader that our current model is limited to an isothermal plasma, and does not include additional effects such as e.g. stratification and loop geometry. Finally, we point out that increasing the value of the viscosity coefficient further does not alter the characteristics of the plasma, unlike increasing the thermal ratio d, when considering thermal conduction. The perturbations continue to propagate with the adiabatic sound speed but will be damped quicker as the viscosity increases.

4. Applications

In this section, we apply the results described above to two specific examples of recently observed oscillations in solar coronal loops, which were both interpreted in terms of slow magneto-acoustic waves.

4.1. Propagating waves observed by TRACE

Firstly, we consider density disturbances observed by TRACE in the lower part of coronal loops. The majority of the propagating disturbances were found in the footpoints of large, diffuse coronal loop structures, close to active regions and they appeared to be a widespread, regularly occurring coronal phenomena (De Moortel et al. 2002a). The propagation speeds were estimated to be of the order of $v \approx 122 \pm 43$ km s^{-1}. The amplitudes of the intensity oscillations were roughly $4.1 \pm 1.5\%$ of the background loop brightness, with the smallest amplitudes detected above a 99% confidence level of the order of 1%. The propagating disturbances were found to be damped very quickly and typically only present in the first 2.9–23.2 Mm along the loop. Loops that were situated above sunspot regions displayed intensity oscillations with periods centred around 3 min, whereas oscillations in "non-sunspot" loops showed periods centred around 5 min.

In Sect. 3, we showed that, for a fixed frequency, there is a minimum damping length that can be obtained due to thermal conduction alone. This value occurs for a thermal ratio $d = 0.1$, which is about four times the value obtained using the typical coronal parameters quoted in Eq. (21). As pointed out above, the intensity oscillations are no longer detected, above a 99% confidence level, when the amplitudes have decreased by a factor of about four. Therefore, rather than a damping length, we will estimate a "detection" length, where the density perturbations have decreased by a factor of four. Figure 7a shows a contour plot of the perturbed density as a function of the length along the loop (in Mm) and time (in minutes), for the

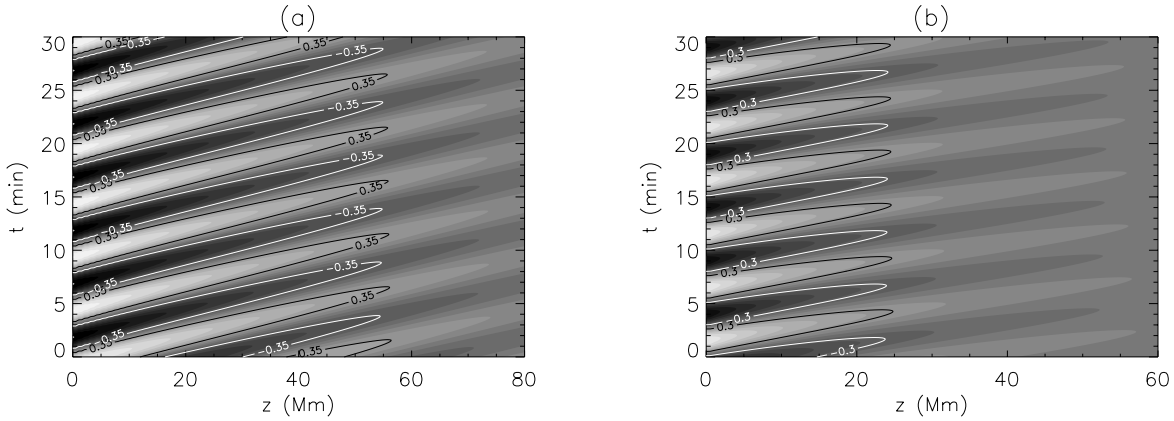

Fig. 7. a) Contour plot of the perturbed density as a function of z and t, for which $d = 0.1$, $\epsilon = 0$ and for which the boundary was driven continuously. **b)** Similar to **a)** but with $d = 0.1$ and $\epsilon = 0.045$.

"enhanced" thermal ratio, $d = 0.1$. The contour level where the density has decreased to a quarter of its initial value is outlined seperatly. We see that in this case, the perturbations would have been detected up to 55–60 Mm along the loop. Using the standard thermal ratio, $d = 0.025$, resulted in a detection length of about 130 Mm. Due to the increased thermal conduction, the temperature perturbations when $d = 0.1$ are considerable smaller compared to $d = 0.025$. Also, although not quite at the isothermal sound speed yet, the perturbations travel somewhat slower for $d = 0.1$. However, the observed propagation speeds, $v \approx 122 \pm 43$ km s^{-1}, overlap with both the isothermal and adiabatic sound speed at 10^6 K, and therefore do not allow us to distinguish between different values of the thermal ratio. Figure 7b shows the combined effect of thermal conductivity and compressive viscosity. For these simulations, the increased value of the thermal ratio, $d = 0.1$, was used, together with an enhanced (by a factor of about 50) viscosity coefficient, $\epsilon = 0.045$. For these values, a detection length of 20–25 Mm, which would correspond with the largest of the observed values, can be obtained. Including the standard value for the viscosity coefficient had no noticeable effect on the damping length. Only taking into account compressive viscosity, the viscosity coefficient has to be increased by a factor of about 115 to obtain this detection length. Seeing there is a minimum damping length that can be achieved by thermal conduction, the value of 25 Mm cannot be reproduced by including thermal conductivity alone.

Although the detection lengths obtained from the simulations are still somewhat larger than the observed values, they are in good order-of-magnitude agreement, especially if we keep in mind that the observed detection lenghts are probably a lower limit due to projection effects. Seeing that we could obtain these detection lengths for "normal" values of the thermal ratio, but only for enhanced values of the viscosity coefficient, it seems appropriate to suggest that the observed density perturbations are largely damped by thermal conduction, with a smaller contribution from compressive viscosity.

4.2. Standing waves observed by SUMER

The second set of oscillations we consider are Doppler shift oscillations observed in hot, active region, coronal loops by SUMER/SOHO (Kliem et al. 2002; Wang et al. 2002a,b). These authors studied a total of 35 cases, associated with 17 flare-like events and estimated the oscillatory periods to be of the order of 10.8–31.1 min. The Doppler shifts were only detected in hot flare lines, at a temperature of $T = 6$–10 MK. In most cases, the oscillations showed a large initial pulse, with amplitudes up to $v = 200$ km s^{-1} and, subsequently, a very rapid damping, with damping times in the range of 5.5–28.9 min. Wang et al. (2002a,b) found good agreement between the observed periods and the theoretically predicted theory of a slow mode, standing wave. The 1/4-period phase difference between Doppler shift and intensity oscillations observed by Wang et al. (2003) provides strong support for the interpretation in terms of slow, standing waves. We will compare our results with those of Ofman & Wang (2002), who model the oscillations in terms of slow magneto-acoustic waves and also include dissipation by thermal conduction and compressive viscosity. The results of the simulations by Ofman & Wang (2002) corresponded well with the observed parameters, hence confirming the interpretation in terms of a slow magneto-acoustic wave.

To model these observations, we will simulate standing waves, by assuming $f(t) = 0$ and considering an initial profile, $F(z)$,

$$v_1(z, 0) = V_0 \sin\left(\frac{2\pi z}{z_{\max}}\right), \tag{22}$$

where V_0 is the (dimensionless) initial amplitude of the wave at $t = 0$. For our simulation, we will use the same loop parameters as Ofman & Wang (2002): a loop length $L = z_{\max} = 400$ Mm, a density $\rho_0 = 8.35 \times 10^{-13}$ kg m^{-3} and a temperature $T_0 = 8 \times 10^6$ K. Using these values for temperature and density, we find a sound speed $c_s \approx 430$ km s^{-1}. Assuming an initial amplitude of about 86 km s^{-1}, gives $V_0 = 0.2$. Using $c_s = 430$ km s^{-1} results in a timescale $\tau = 15.5$ min, a thermal ratio $d = 0.36$ and a dimensionless viscosity coefficient $\epsilon = 0.013$. We note that this value of the thermal ratio corresponds to more than three times the value $d_{\min}$, where the damping due to thermal conduction reaches its minimum. For this value of d, we expect the perturbations to travel at some hybrid speed, somewhere between the adiabatic and isothermal sound speed, $c_i \approx 330$ km s^{-1}. A cross-section of the

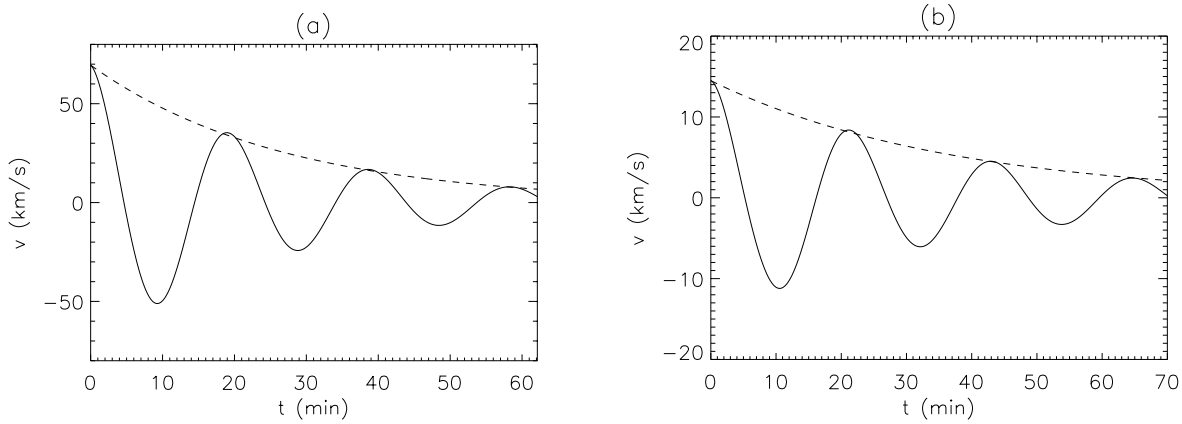

Fig. 8. a) A cross-section of the perturbed velocity as a function of time at $z = 140$ Mm, for $T = 8$ MK and $V_0 = 0.2$. The exponential decay is shown as a dashed line. **b)** Similar to **a)** but with $T = 6.3$ MK and $V_0 = 0.047$.

perturbed velocity as a function of time at $z = 140$ Mm is shown in Fig. 8a. The fact that the period of the perturbed velocity, $P = 19$ min, is not equal to the timescale, $\tau = 15.5$ min, demonstrates that the wave does not travel at the adiabatic sound speed, but at a slower hybrid speed. Indeed, if the perturbations travelled at exactly the isothermal sound speed, the simulated (or isothermal) period would have been $\tau\sqrt{\gamma} = 20$ min. Fitting an exponential decay (dashed line) of the form $V_0 \exp(-t/t_d)$ to the velocity perturbations gives a damping time t_d of the order of 26.5 min. Due to the high value of the thermal conductivity, the temperature perturbations are very small, of the order of 3% of the background temperature.

To model the recent example observed by Wang et al. (2003), we decrease the temperature to $T = 6.3 \times 10^6$ K, which results in a sound speed $c_s \approx 380$ km s^{-1}, a timescale $\tau = 17.5$ min, a thermal ratio $d = 0.23$ and a dimensionless viscosity coefficient $\epsilon = 0.008$. Setting $V_0 = 0.047$ gives an initial amplitude of about 18 km s^{-1}. The result of this simulation is shown in Fig. 8b, again as a cross-section of the perturbed velocity. The period of the oscillation is about 21 min (the "isothermal" period is 22.6 min in this case) and the damping time, given by the exponential decay, is 36.7 min.

For the $T = 8$ MK case, the obtained damping time $t_d = 26.7$ min, is longer than the value obtained by Ofman & Wang (2002), who obtain a damping time of 17.7 min. However, these authors include non-linearity and viscous heating in their model, which could explain the difference in the obtained damping times. The results of the simulations for $T = 6.3$ MK, on the other hand, do agree well with the recent example presented by Wang et al. (2003), who quoted a damping time of 36.8 min. The main result of our study is that the perturbations do not oscillate with the "adiabatic" period, but with a period which could be up to a factor $\sqrt{\gamma}$ longer.

5. Discussion and conclusions

In this paper, we have investigated the propagation and damping of slow magneto-acoustic waves in a homogeneous medium, including the effects of thermal conduction and compressive viscosity. Varying the dimensionless parameters revealed the complex behaviour of slow modes under different physical circumstances. Although MHD waves have been studied extensively in the past, pointing out all the properties of slow magneto-acoustic waves is useful, given the recent amount of observations that have been interpreted in terms of slow waves. We found that including thermal conduction introduces the "thermal" mode. When considering standing waves, i.e. keeping the wavenumber k real and fixed, the thermal mode is purely decaying in time. If the thermal ratio d tends to zero, the thermal mode becomes isobaric, i.e. there are no pressure perturbations. If the thermal ratio d tends to infinity, there are no density perturbations. For propagating waves, i.e. keeping the frequency ω real and fixed, the thermal mode is oscillatory and decaying. Depending on the boundary conditions, perturbations will be a combination of both the slow and the thermal mode. We showed that there is a minimum damping time (or length) that can be obtained by thermal conduction alone, so if stronger damping is required, an alternative mechanism such as compressive viscosity has to be included. Indeed, including a large amount of thermal conductivity significantly alters the characteristics of the medium. The plasma becomes isothermal almost instantaneously and the perturbations propagate largely undamped, at the slower, isothermal sound speed. The different speed results in a change in the resonant behaviour, with resonance occurring for different loop lengths, compared to the ideal case. For a coronal plasma at a temperature of 1 MK, thermal conduction appears to be the dominant damping mechanism. We had to increase the compressive viscosity coefficient by a factor of ten to one hundred to obtain a noticeable effect on the waves. Including "normal" thermal conduction or strongly enhanced compressive viscosity produced largely similar results.

In Sect. 4, we considered two different types of recently observed oscillations, namely propagating and standing slow magneto-acoustic waves. In case of the propagating density perturbations, thermal conduction alone resulted in a detection length of 55–60 Mm, which is in good order-of-magnitude agreement with observed values (3–23 Mm), given that these are probably a lower limit due to projection effects. Combining thermal conduction with enhanced compressive viscosity (by a factor of 50) produced a detection length of roughly 20−25 Mm, which agrees with the observations

without considering potential projections effects. Given that these are propagating perturbations, in which case the thermal mode would be oscillatory, it might be possible to obtain faster damping by choosing the right boundary conditions so that the perturbations consist mainly of the thermal mode. Secondly, rapidly damped Doppler shift oscillations, observed in hot coronal loops, were modelled as standing waves. Due to the high temperatures, a large amount of thermal conductivity is present, which results in the perturbations oscillating with a slower, hybrid period. The damping time we obtained for $T = 8$ MK and $V_0 = 0.2$ is slightly longer than the value obtained by Ofman & Wang (2002). However, for $T = 6.3$ MK and $V_0 = 0.047$, we find good agreement with a more recently observed example (Wang et al. 2003). Nakariakov et al. (2000) point out that non-linearity does not play an important role in the dissipation of waves with initial amplitudes less than 8−10%. This could explain why we find good agreement for the case with a very small initial amplitude.

To eliminate any other effect on the wave propagation, we restricted our model to motions along a constant background magnetic field to study the effects of thermal conduction and compressive viscosity. However, a more realistic model would have to include several other effects. Firstly, including gravity along the loop could be considered and would probably result in an additional effect on the damping of the perturbations. Secondly, the model could be extended to two dimensions to include effects such as the configuration of the background magnetic field, the geometry of the coronal loops (curvature) and a density profile that is inhomogeneous across the loop. Such a density profile could result in phase mixing or resonant absorption, which would again influence the wave damping. Including non-linearity and non-uniformity would result in the excitation of different MHD modes, such as fast waves, and energy could leave the system via this mode coupling. Also, a resonant layer could exist inside the loop due to the inhomogeneous density profile. All these effects are likely to cause additional dissipation and hence result in shorter damping times or lengths.

References

Aschwanden, M. J., Fletcher, L., Schrijver, C. J., & Alexander, D. 1999, ApJ, 520, 880

Aschwanden, M. J., De Pontieu, B., Schrijver, C. J., & Title, A. 2002, Sol. Phys., 206, 99

Berghmans, D., & Clette, F. 1999, Sol. Phys., 186, 207

Brynildsen, N., Maltby, P., Fredvik, T., & Kjeldseth-Moe, O. 2002, Sol. Phys., 207, 259

DeForest, C. E., & Gurman, J. B. 1998, ApJ, 501, L217

De Moortel, I., Ireland, J., & Walsh, R. W. 2000, A&A, 355, L23

De Moortel, I., Ireland, J., Hood, A. W., & Walsh, R. W. 2002a, Sol. Phys., 209, 61

De Moortel, I., Hood, A. W., Ireland, J., & Walsh, R. W. 2002b, Sol. Phys., 209, 89

De Moortel, I., Ireland, J., Hood, A. W., & Walsh, R. W. 2002c, A&A, 387, L13

De Pontieu, B., Martens, P. C. H., & Hudson, H. S. 2001, ApJ, 558, 859

Field, G. B. 1965, ApJ, 142, 531

Goossens, M., Andries, J., & Aschwanden, M. J. 2002, A&A, 394, L39

Hollweg, J. 1985, J. Geophys. Res., 90, 7620

Hood, A. W., Van der Linden, R., & Goossens, M. 1989, Sol. Phys., 120, 261

Hood, A. W., & Priest, E. R. 1980, A&A, 87, 126

Kliem, B., Dammasch, I. E., Curdt, W., & Wilhelm, K. 2002, ApJ, 568, L61

Nakariakov, V. M., Ofman, L., DeLuca, E. E., Roberts, B., & Davila, J. M. 1999, Science, 285, 862

Nakariakov, V. M., Verwichte, E., Berghmans, D., & Robbrecht, E. 2000, A&A, 362, 1151

Nakariakov, V. M., & Ofman, L. 2001, A&A, 372, L53

Ofman, L., Romoli, M., Poletto, G., Noci, C., & Kohl, J. L. 1997, ApJ, 491, L111

Ofman, L., Nakariakov, V. M., & DeForest, C. E. 1999, ApJ, 514, 441

Ofman, L., Romoli, M., Poletto, G., Noci, C., & Kohl, J. L. 2000, ApJ, 529, 592

Ofman, L. 2002, ApJ, 568, L135

Ofman, L., & Aschwanden, M. J. 2002, ApJ, 576, L153

Ofman, L., & Wang, T. J. 2002, ApJ, 580, L85

O'Shea, E., Muglach, K., & Fleck, B. 2002, A&A, 387, 642

Porter, L. J., Klimchuk, J. A., & Sturrock, P. A. 1994, ApJ, 435, 482

Porter, L. J., Klimchuk, J. A., & Sturrock, P. A. 1994, ApJ, 435, 502

Robbrecht, E., Verwichte, E., Berghmans, D., et al. 2001, A&A, 370, 591

Roberts, B., Edwin, P. M., & Benz, A. O. 1984, ApJ, 279, 857

Roberts, B. 1985, in Solar System Magnetic Fields, ed. E. R. Priest (Dordrecht: Reidel), Chap. 3

Roberts, B. 2000, Sol. Phys., 193, 139

Ruderman, M., & Roberts, R. 2002, ApJ, 577, 475

Schrijver, C. J., Title, A. M., Berger, T. E., et al. 1999, Sol. Phys., 187, 261

Schrijver, C. J., & Brown, D. S. 2000, ApJ, 537, L69

Schrijver, C. J., Aschwanden, M. J., & Title, A. 2002, Sol. Phys., 206, 69

Stein, R. F., & Spiegel, E. A. 1967, J. Acous. Soc. Am., 42, 866

Tsiklauri, D., & Nakariakov, V. M. 2001, A&A, 379, 1106

Wang, T. J., Solanki, S. K., Curdt, W., Innes, D. E., & Dammasch, I. E. 2002a, ESA-SP, 508, 465

Wang, T. J., Solanki, S. K., Curdt, W., Innes, D. E., & Dammasch, I. E. 2002b, ApJ, 574, L101

Wang, T. J., Solanki, S. K., Innes, D. E., Curdt, W., & Marsh, E. 2003, A&A, 402, L17